ELSEVIER

Journal of Molecular Catalysis A: Chemical 176 (2001) 127–139

JOURNAL OF MOLECULAR CATALYSIS A: CHEMICAL

www.elsevier.com/locate/molcata

The role and stability of Li_2O_2 phase in supported LiCl catalyst in oxidative dehydrogenation of *n*-butane

M.V. Landau [a,*], A. Gutman [a], M. Herskowitz [a], R. Shuker [b], Y. Bitton [b], D. Mogilyansky [c]

[a] *Chemical Engineering Department, The Blechner Center for Industrial Catalysis and Process Development, Ben-Gurion University of the Negev, P.O. Box 653, Beer-Sheva 84105, Israel*

[b] *Department of Physics, Ben-Gurion University of the Negev, Beer-Sheva 84105, Israel*

[c] *Institutes of Applied Research, Ben-Gurion University of the Negev, Beer-Sheva 84105, Israel*

Received 31 January 2001; received in revised form 12 April 2001; accepted 25 May 2001

Abstract

This study was aimed at defining the role of active phases in supported LiCl and LiCl–$DyCl_3$ catalysts in the catalytic oxidative dehydrogenation (ODH) of *n*-butane. LiCl supported on silica displayed the highest activity and selectivity in *n*-butane ODH compared with other alkali metal halides. Addition of $DyCl_3$ increased the activity. TPO, XRD and Raman light scattering (RLS) data showed that LiCl and $DyCl_3$ formed during the preparation stage were converted to Li_2O_2 and DyOCl phases, respectively, by calcination in air at >400°C. The results of separate TPR experiments (O_2-oxidation–butane reduction) along with XRD, RLS and X-ray photoelectron spectroscopy (XPS) data proved that butane reacts mainly with oxygen species of Li_2O_2 phase at ODH conditions, probably attributed to $[Li^+O^-]$ pairs. The proposed functions of chlorine and dynamic oxygen in the ODH of butane are consistent with the activity, selectivity and stability of silica and magnesia-supported catalysts. High thermal stability of Li_2O_2 in oxidized LiCl catalyst was attributed to the formation of protective $Li_2O{\cdot}LiCl$ surface layer. Deactivation of LiCl/SiO_2 catalyst in *n*-butane ODH is caused by the formation of Li-silicates at reaction conditions while LiCl/MgO display a stable performance.

Keywords: Oxidative dehydrogenation; *n*-Butane; Lithium peroxide; SiO_2; MgO-supported catalyst; XRD; XPS; Raman scattering spectroscopy

1. Introduction

The exothermic process of oxidative dehydrogenation (ODH) of light paraffins is a viable alternative to endothermic catalytic dehydrogenation and steam cracking for light olefins production. A large number of catalyst formulations were tested in ODH of C_2–C_4 paraffins over the last three decades. The best performance displayed noble metal catalysts at 700–1000°C working at short millisecond contact times [1–6] and alkaline-earth-based metal-oxide catalysts [7,8], especially halogen-promoted [8–11]. Halogenated and particularly chlorinated catalysts containing lithia, rare or alkaline-earth oxides or halides, bulk or supported on magnesia, zirconia or alumina displayed the best performance at relatively low temperatures of <600°C [9–11]. A Li–MgO–$Dy(Ce)_2O_3$–Cl formulation, introduced by Conway et al. [12] for ODH of

* Corresponding author. Tel.: +972-8-6472141; fax: +972-8-6477678.
E-mail address: mlandau@bgumail.bgu.ac.il (M.V. Landau).

1381-1169/01/$ – see front matter
PII: S1381-1169(01)00241-2

ethane yielded excellent performance (62 wt.% ethylene yield, 76 wt.% selectivity at 570°C). Subsequent studies of Landau et al. [11,13] demonstrated high efficiency of this catalytic system in oxidative conversion of LPG (mixture of propane, butane and isobutane). Experiments carried out at 580–600°C and O_2 to LPG molar ratio of unity on Li–MgO–$Dy(Ce)_2O_3$–Cl catalysts yielded 45–50 wt.% C_2–C_4 olefins and 65–75 wt.% selectivity. Other halogens F, Br and I yielded inferior results. Similar catalysts supported on zirconia produced olefins at much higher rate [13,14]. As was shown in [13], chlorine is a key component determining the activity level of MgO- or ZrO_2-based Li–RE-oxide catalysts in LPG ODH. Recently, it was demonstrated that pure LiCl supported on SiO_2 [15] or ZrO_2 [16] display better performance in ethane ODH, 68% ethylene yield at 70% selectivity (LiCl/ZrO_2, 650°C) and 79.2% ethylene yield at 80% selectivity (LiCl/SiO_2, 600°C), but the stability of these catalysts was relatively low.

Defining the role of active phases in supported LiCl and LiCl–RE-chloride catalysts and their behavior in ODH catalytic reactions is a basis for better understanding of the nature of catalytic action and development of new efficient ODH catalysts. It is known that LiCl is not stable in oxidative atmosphere at high temperature forming Li-peroxide phase. Appearance of Li-peroxide phase after exposure of supported LiCl to oxygen was reported by Gutman et al. [17] for LiCl/SiO_2 (XRD), Wang et al. [16] for LiCl/ZrO_2 (XRD) and recently by Bothe-Almquist et al. [18] for LiCl/MgO (XRD, XPS, EPR). But it is not clear if the catalytic cycle of light paraffins ODH is directly connected with formation–decomposition of this phase. Since pure bulk Li_2O_2 decomposes at >194°C [19,20], it is doubtful that it can play a role of active phase in paraffins ODH at $\geq$550°C. Furthermore, the mechanism of supported LiCl deactivation and chlorine loss by chemical phase transformations in ODH conditions should be defined better as a basis for minimizing the chlorine and HCl evolution preventing corrosion problems in light paraffins ODH processing.

The objective of this study was to define the oxide phases and chlorine compounds formed from LiCl and $DyCl_3$ in supported metal-chloride catalysts at ODH conditions, their transformations in *n*-butane ODH, type of catalytically active oxygen in these phases and deactivation mechanism. For this purpose, the oxygen consumption/release, phase composition and the state of surface oxygen at different stages of redox cycle with supported LiCl and LiCl–$DyCl_3$ catalysts were measured by TPO–TP-reaction, XRD, Raman light scattering (RLS) and X-ray photoelectron spectroscopy (XPS) methods. The data of catalysts performance, TPO–TP-reaction experiments and species identified by XRD, XPS and RLS are in agreement with a model assuming chlorine-modified Li_2O_2 as an active phase in *n*-butane ODH.

2. Methods

2.1. Catalysts preparation

The LiCl/SiO_2, LiCl/MgO, $DyCl_3$/SiO_2 and LiCl–$DyCl_3$/SiO_2 catalysts were prepared by impregnation of corresponding support with aqueous solution of metal-chloride salt. Aqueous slurry was prepared by mixing powdered silica (Celite with surface area of 31 m^2/g) or MgO (surface area 25 m^2/g) with aqueous solution (water to MgO or SiO_2 weight ratio of 2) of LiCl and/or $DyCl_3 \cdot 6H_2O$ salts (all from Aldrich). Then evaporation and drying at 120°C for 5 h and calcination at 550°C for 16 h were carried out. The chemical composition of impregnated catalysts was varied over a wide range.

2.2. Catalysts characterization

The catalysts composition was measured by energy-dispersive X-ray (EDAX)-JEM-35, JOEL, link system AN-1000, Si–Li detector. The surface area was determined using BET method (N_2-adsorption, NOVA-1000 Quantachrome, version 5.01). Phase composition was measured on XRD Philips PW 1050/70 equipped with a long, fine focus Cu anode tube, 40 kW, 28 mA, a scintillation detector and a diffracted beam monochromator. The phase identification was carried out according to JCPDS-ICDD powder diffraction cards. The quantity of amorphous phase was estimated from the ratio of integrated intensities of amorphous hallo and selected diffraction peaks. PHI 549 SAM/AES/XPS apparatus with double CMA and Mg Kα X-ray source has been used for XPS measurements of the catalysts. After recording general survey spectra, high-resolution scans were taken at

25 eV for O 1s peaks. The spectral components of O signals were found by fitting a sum of single component lines to the experimental data by means of nonlinear least-square, curve-fitting to Gauss–Lorentz shape function using software for peaks deconvolution. The quantitative distribution of oxygen atoms with different O 1s characteristics as well as total atomic surface concentration accounted for the sensitivity factor of all detected elements. Binding energies were referred to the carbon 1s line at 284.5 eV. The TPO and TP-reaction measurements were carried out in AMI-100 catalyst characterization system (Zeton-Altamira) equipped with quadroupole mass spectrometer (Ametek-1000). Raman scattering was used to determine the presence of Li_2O_2 phase. The Raman spectra were recorded on a system of Ar^+ laser at 480 nm for excitation and Spex double monochromator 1401 with a cooled PM to −20°C. An A/D converter was employed to obtain the spectra on a PC for data collection and analysis.

Care was taken to avoid contact of samples, especially those containing chlorine, with air. After calcination, the samples were cooled in air to 150–200°C and immediately transferred to a glove box. There they were crushed, sieved to 20–40 mesh for catalytic tests or pressed into 10 mm disks for recording the Raman spectra and XPS measurements or loaded to a sample holder for recording the XRD patterns. The XRD and Raman spectra were recorded within less than 20 min. Exposing the samples to air at room temperature for longer periods, caused substantial changes of corresponding spectra due to adsorption of moisture.

2.3. Catalysts testing

A tubular titanium reactor, 17 mm ID and 250 mm length, supplied with central thermowell was used for the catalyst tests. The reactor was heated by electric heat tape. Butane, oxygen and nitrogen were fed separately by mass flow controllers (Brooks Instrument) and mixed in preheater at 450°C. The catalyst was loaded in the reactor between two layers of quartz pellets. Less than 5% *n*-butane conversion was measured in the titanium reactor packed with quartz due to homogeneous reaction over the range of operating conditions in this study. Titanium reactor displayed the lowest contribution of homogeneous reactions, mostly combustion, among several tested materials. The analysis of dried reaction products was performed on line with GC HP-5890 that contained four columns and two detectors TCD and FID controlled by ChemStation analytical software [13].

3. Results and discussion

3.1. Performance of halide catalysts in n-butane ODH

3.1.1. Effect of metal-halide nature

Since the nature of metal and halide strongly affects the performance of supported metal-halide catalysts in ODH reactions [9,15], comparative catalytic performance study of four Li-halides and four alkali metal chlorides in oxidation of *n*-butane at 550°C were conducted. The most efficient catalytic system was selected for further investigation. Silica support was used in this case because its own activity in *n*-butane oxidation at selected conditions was negligible. Two series of catalyst samples were prepared by impregnation of silica with aqueous solutions of alkali halides followed by evaporation of water excess, drying and calcination at 550°C for 16 h. All the samples before calcination contained 50 wt.% alkali halides. Butane conversion and olefins selectivity, compared after 0.25 and 2 h on stream, are listed in Table 1. LiCl displayed the best performance in terms of activity, selectivity and stability. Other catalysts yielded lower activity (LiF, LiI, RbCl and CsCl) or lower selectivity (LiBr and NaCl). KCl yielded similar activity and selectivity, but the stability was lower. Actually, all alkali-halides displayed low stability, except LiCl.

3.1.2. Effect of LiCl loading

The effect of LiCl loading on performance of SiO_2- and MgO-supported catalysts in *n*-butane ODH is shown in Fig. 1. The two supports displayed different behavior: highest olefins yield and productivity, at those operating conditions, was measured with catalysts containing 50 wt.% LiCl on SiO_2 and 10 wt.% LiCl on MgO. This difference in optimal LiCl loadings at similar surface areas could be explained by different distribution of active component in the pores. The surface area of calcined LiCl/SiO_2 catalyst gradually decreased from 12 to 6.5 m^2/g by increasing the

Table 1
Performance of supported alkali halogens in *n*-butane ODH (testing conditions: $T = 550^{\circ}C$; $WHSV_{n\text{-}C_4} = 0.5\,h^{-1}$; feed composition (mol%): *n*-butane = 20, oxygen = 20, nitrogen = 60)

Metal	Halogen	*n*-Butane conversion (wt.%)		Olefins selectivity (wt.%)	
		$t = 0.25$ h	$t = 2.0$ h	$t = 0.25$ h	$t = 2.0$ h
Li	F	13	11	69	72
Li	Cl	29	29	75	76
Li	Br	35	23	40	43
Li	I	6	4	47	51
Na	Cl	35	33	65	65
K	Cl	28	26	72	72
Rb	Cl	19	16	74	75
Cs	Cl	18	15	75	77

LiCl loading in the range 10–50 wt.%, while at 75% LiCl it dropped to 0.6 m^2/g. In the case of LiCl/MgO, the surface area of calcined catalyst was 17 m^2/g at 10 wt.% LiCl loading, dropped to 8 m^2/g at 20 wt.% LiCl. At optimal LiCl loading, the MgO-based catalyst displayed 25% higher *n*-butane conversion at slightly lower olefins selectivity compared with SiO_2-based catalyst.

Based on this data, five catalyst samples containing LiCl on silica, LiCl on magnesia, LiCl–$DyCl_3$ on silica at optimal LiCl loadings and comparative Li_2O and $DyCl_3$ on silica catalysts were selected for further investigation of their stability and phase transformations. The compositions and surface areas of selected catalysts are summarized in Table 2.

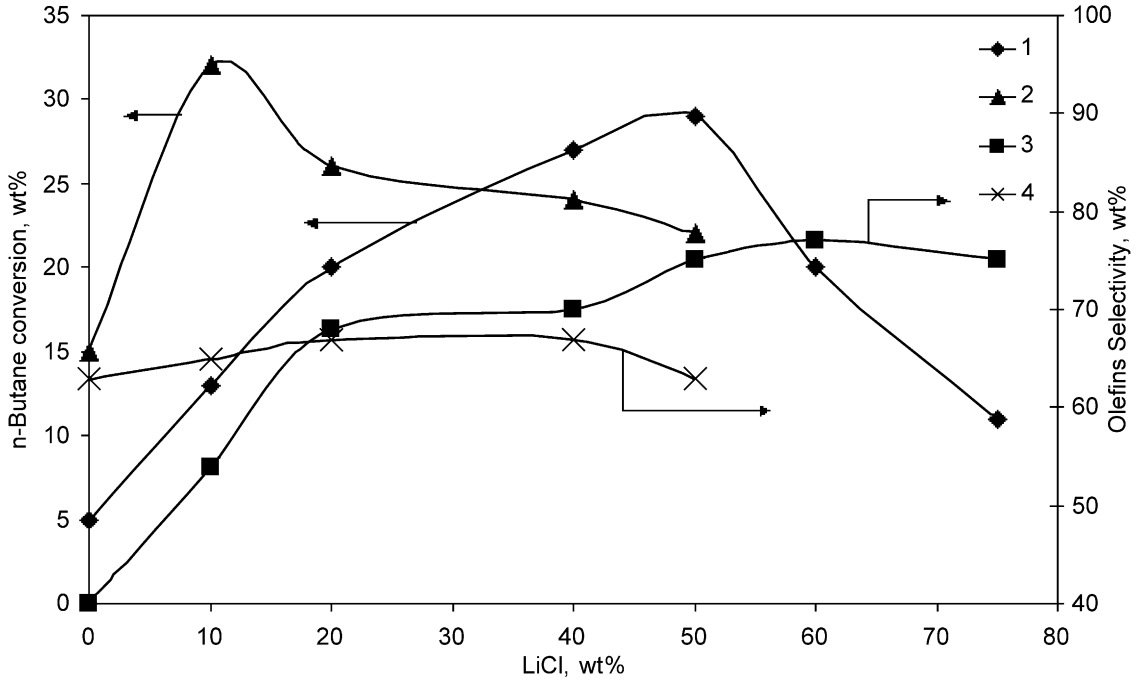

Fig. 1. Effect of LiCl loading on the performance of $LiCl/SiO_2$ and LiCl/MgO catalysts ($T = 550^{\circ}C$, $WHSV_{n\text{-}C_4} = 0.5\,h^{-1}$, molar feed ratio $n\text{-}C_4{:}O_2{:}N_2 = 1{:}1{:}3$): *n*-butane conversion — (1) $LiCl/SiO_2$, (2) LiCl/MgO; olefins selectivity — (3) $LiCl/SiO_2$, (4) LiCl/MgO.

Table 2
Properties of supported catalysts

SiO_2/MgO supported catalysts	Chemical composition (wt.%)			Surface area (m^2/g)
	LiCl	Li_2O	$DyCl_3$	
LiCl/MgO	10.0	–	–	17
LiCl/SiO_2	50.8	–	–	6.5
Li_2O/SiO_2	–	33.2	–	7.9
$DyCl_3$/SiO_2	–	–	49.9	6.9
LiCl–$DyCl_3$/SiO_2	39.0	–	33.7	6.0

3.1.3. Stability of LiCl/SiO_2 and LiCl–$DyCl_3$/SiO_2 catalysts

LiCl and LiCl–$DyCl_3$ on silica were prepared by impregnation followed by drying at 120°C and further calcination in air at 500°C. The chemical composition of the catalysts after drying was equal to the expected value from preparation conditions. The Li/Si atomic ratio in both catalysts before and after calcination corresponded to optimal LiCl loading. However, significant chlorine loss was recorded after calcination in air at 550°C (70% for LiCl and 25% for LiCl–$DyCl_3$) as listed in Table 3. This could be evident for partial transformation of Li- and Dy-chlorides at high calcination temperature in air due to decomposition or oxidation causing chlorine loss. Activity and stability of both catalysts after calcination at 550°C were tested in butane ODH (Table 4). Addition of $DyCl_3$ to optimized LiCl/SiO_2 catalyst yielded an increase of *n*-butane conversion by 10–17% with slight decrease of olefins selectivity. LiCl–$DyCl_3$/SiO_2 lost 32 wt.% Cl after 2 h on stream at 550°C, in contrast to little loss for LiCl/SiO_2, while no significant deactivation was recorded in both cases. Deactivation and chlorine loss at extremely fast rate were recorded for LiCl/SiO_2 and LiCl–$DyCl_3$/SiO_2 at 600°C.

Substantial chlorine loss in supported LiCl and LiCl–$DyCl_3$ catalysts during calcination and catalytic oxidative conversion of *n*-butane at fixed metal/silica ratio is evident for oxidative transformations of metal-chloride phases. These transformations lead to the

Table 3
Chemical composition of LiCl/SiO_2 and LiCl–$DyCl_3$/SiO_2 catalysts

Catalyst	Chemical composition						Chlorine loss during calcination (wt.%)
	After drying at 120°C, air			After calcination at 550°C, air			
	Li/Si	Dy/Si	Cl/Si	Li/Si	Dy/Si	Cl/Si	
LiCl/SiO_2	2.0	–	2.0	1.9	–	0.6	70
LiCl–$DyCl_3$/SiO_2	2.0	0.3	2.8	2.0	0.28	2.1	25

Table 4
Stability of LiCl/SiO_2 and LiCl–$DyCl_3$/SiO_2 catalysts (testing conditions: $WHSV_{n\text{-}C_4} = 0.5\,h^{-1}$; feed composition (mol%): *n*-butane = 20, oxygen = 20, nitrogen = 60)

Testing temperature (°C)	Run time (h)	*n*-Butane conversion (wt.%)		Olefins selectivity (wt.%)		Chlorine loss (wt.%), 2 h stream	
		LiCl	LiCl–$DyCl_3$	LiCl	LiCl–$DyCl_3$	LiCl	LiCl–$DyCl_3$
550	0.25	29	34	75	69	–	–
550	2.0	29	33	76	69	0	32
600	0.25	64	70	66	65	4	18
600	1.0	59	64	66	66	13	66

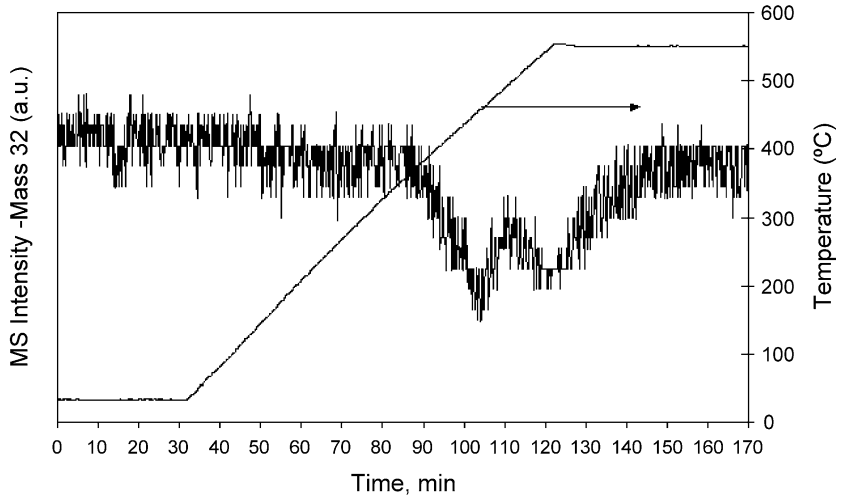

Fig. 2. TPO spectra of 50.0 wt.% $LiCl/SiO_2$ catalyst dried at 120°C.

formation of active phase at calcination step, as well as to catalyst deactivation in catalytic run. In order to clarify the nature, role of these metal-oxide phases and their stability, the $LiCl/SiO_2$ and $LiCl–DyCl_3/SiO_2$ catalysts were investigated after different treatments by TPO, TP-reaction, XRD, RLS and XPS methods.

3.2. Characterization of oxide phases formed by metal-halide oxidation

3.2.1. Oxygen adsorption–desorption cycle in ODH

Temperature-programmed experiments were carried out with 3 g of 50 wt.% $LiCl/SiO_2$ loaded in AMI-100 reactor and a mixture of 5 mol% O_2 in He, fed at 25 cm^3/min. The temperature was gradually increased by 5°C/min up to 550°C. Two peaks of oxygen consumption were measured at 450 and 550°C, shown in Fig. 2. No oxygen consumption was detected with pure silica at the same conditions. This fact and the chlorine release from dried $LiCl/SiO_2$ catalyst during calcination in air at 550°C (Table 2) render the TPO data evident for partial conversion of LiCl to surface oxide compound LiO_x.

Further experiments were carried out with 25 cm^3/min of 9 mol% butane in helium fed to AMI-100 reactor containing 3 g catalyst. The temperature was gradually increased at 5°C/min up to 550°C. Operating conditions were kept constant at the final temperature for 1.5 h, then switched to He. The catalyst was purged for 1 h and cooled to 200°C. Then, the procedure of the first run was repeated. Prior to the third run the catalyst was reoxidized in 5 mol% O_2 in He flow at 550°C for 2 h with subsequent cooling to 200°C. The TP-reaction spectra of the butane consumption for $LiCl/SiO_2$ and $DyCl_3–LiCl/SiO_2$ catalysts are shown in Fig. 3. Figs. 2 and 3 indicate that at selected ODH conditions the full oxidation of LiCl and its reduction with *n*-butane take about 50 min.

$MgO–Dy_2O_3–Li–Cl–O$ adsorbed oxygen reversibly from gas phase at 550°C [13]. This adsorbed oxygen further reacted with butane in the absence of oxygen in gas phase giving the same products distribution as in catalytic test performed with oxygen–butane feed. This behavior was recorded up to full consumption of dynamic-adsorbed oxygen in the catalytic reaction. The reaction cycle was repeated after readsorption of oxygen from gas phase. It was assumed that adsorption of molecular oxygen at the surface of MgO modified by $Dy_2O_3–Li–Cl$ proceeded without redox transformations of metal cations producing strongly nucleophilic oxygen atoms capable of abstracting protons from paraffin molecule. No information about the nature of surface or bulk phases containing this oxygen is available.

The behavior of LiCl and $LiCl–DyCl_3$ supported on silica in thermo-programmed ODH of butane

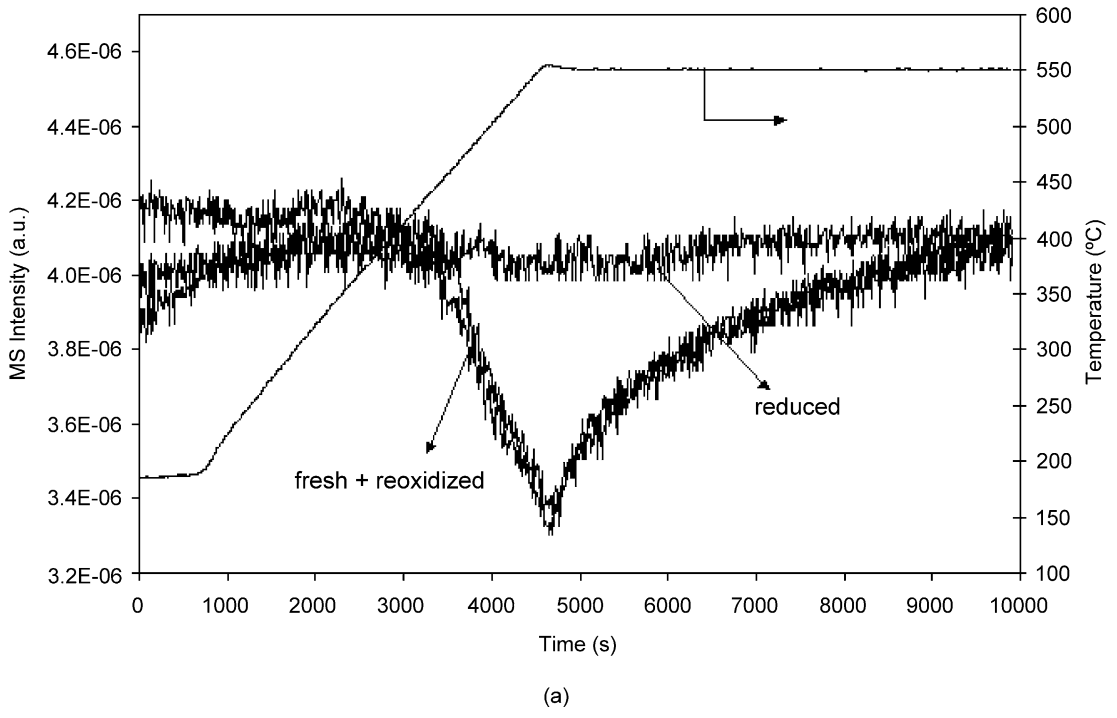

(a)

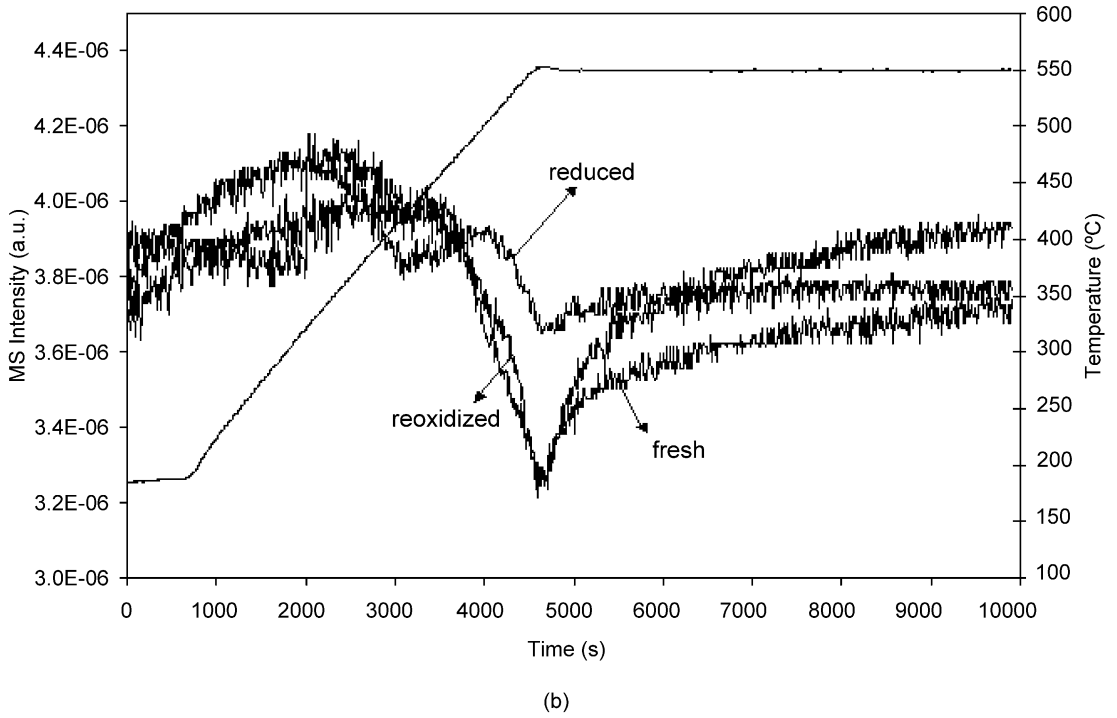

(b)

Fig. 3. TP-reaction spectra of butane oxidation recorded with: (a) 50.0 wt.% $LiCl/SiO_2$; (b) 39.0 wt.% LiCl–33.7 wt.% $DyCl_3/SiO_2$.

measured in this work and of MgO–Dy_2O_3–Li–Cl–O measured in [13], was similar. The distribution of reaction products detected by MS (C_2–C_4 olefins, CO_2, H_2O, H_2) was also similar to that measured in standard catalytic tests. Introduction of $DyCl_3$ to $LiCl/SiO_2$ composition increased the area of TP-reaction peaks (Fig. 3b) in agreement with higher butane conversion measured with oxygen–butane feed (Table 4). It means that the catalytic action of LiCl and $DyCl_3$ phases is directly related to their ability to replace part of chlorine anions with oxygen anions during exposure to molecular oxygen at >400°C. The nature of phases formed by LiCl and $DyCl_3$ oxidation at high temperatures that contain dynamic oxygen is important for understanding the ODH catalytic cycle.

3.2.2. Dynamic oxygen in $LiCl/SiO_2$ and $LiCl–DyCl_3/SiO_2$ catalysts

Formation of new oxide or oxychloride phases in silica-supported Li- and Dy-chlorides, during calcination in air at 550°C through oxygen chemisorption, was studied by XRD. The pattern of pure silica support (Fig. 4A) displays a mixture of amorphous part (∼40%) and crystalline polymorphs of SiO_2, most of it cristobalite (PDF 11-695) and quartz (PDF 33-1161). The amorphous silica part disappeared after deposition of active components due to crystallization and interaction with LiCl (Fig. 4B–F). Deposition of lithium nitrate followed by calcination at 550°C in air (33.2 wt.% Li_2O) yielded formation of three new phases compared with pure support as detected by XRD (Fig. 4B). Two lithium silicates — Li_2SiO_3

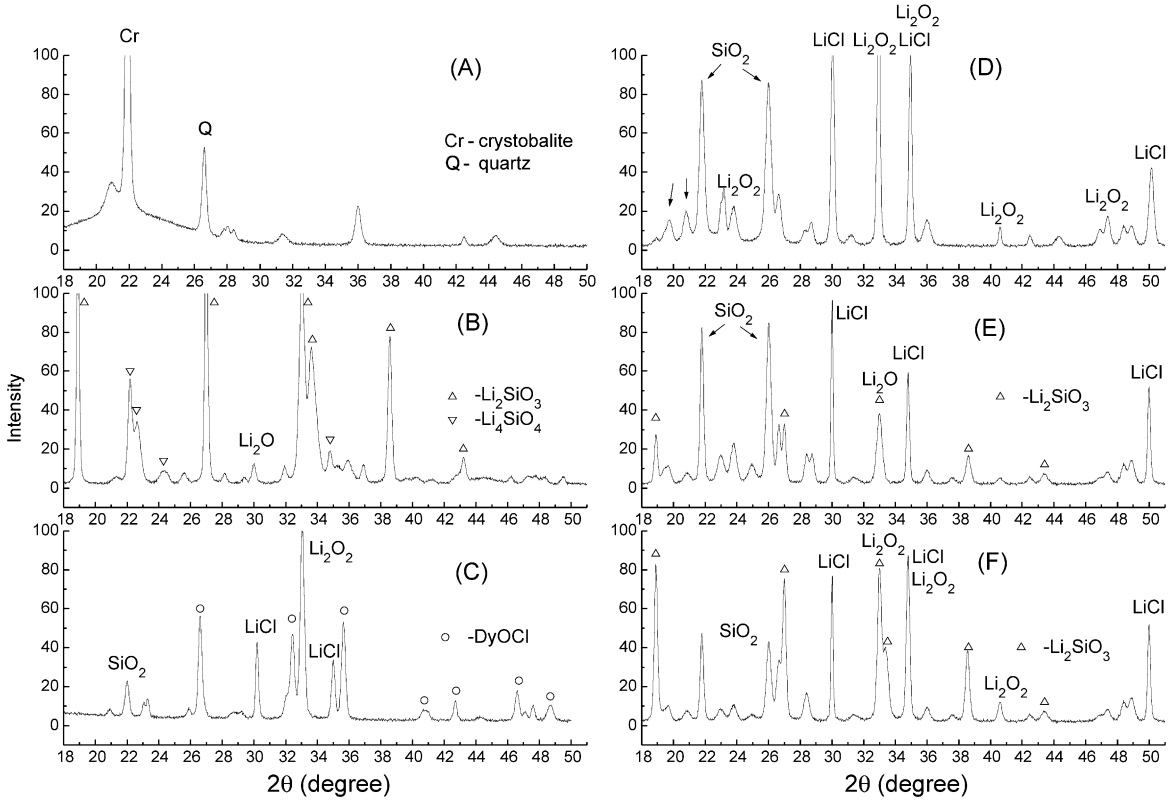

Fig. 4. XRD patterns of silica support and $LiCl–DyCl_3/SiO_2$ catalysts: (A) silica support (Celite); (B) 33.2 wt.% Li_2O/SiO_2 calcined at 550°C; (C) 39.0 wt.% LiCl–33.7 wt.% $DyCl_3/SiO_2$ catalyst calcined in air at 550°C; (D) 50.0 wt.% $LiCl/SiO_2$ catalyst calcined in air at 550°C; (E) 50.0 wt.% $LiCl/SiO_2$ catalyst calcined in air at 550°C and reduced by n-C_4H_{10} at 550°C; (F) 50.0 wt.% $LiCl/SiO_2$ catalyst calcined in air at 550°C, reduced by n-C_4H_{10} at 550°C and reoxidized in air at 550°C.

(PDF 29-829) and Li_4SiO_4 (PDF 20-637) and a small amount of Li_2O (PDF 12-254) were detected. It means that part of lithium oxide produced at the surface of silica by decomposition of $LiNO_3$ during calcination reacted with the support yielding Li-silicate phases, so that peaks corresponded to quartz and cristobalite almost completely disappeared.

The XRD pattern of the catalyst containing two chloride phases deposited on silica (39 wt.% LiCl — 33.7 wt.% $DyCl_3/SiO_2$) after calcination in air at 550°C is shown in Fig. 4C. Two crystalline phases containing lithium-chloride (LiCl) (PDF 4-664) and lithium peroxide (Li_2O_2) (PDF 9-355) were detected. Lines, with characteristics of $DyCl_3$ phase are absent, since during calcination in air, it was converted to Dy-OCl (PDF 22-260). In spite of comparatively low silica content in this sample, diluted by Li–Dy-compounds, cristobalite and quartz was still observed but no peak characteristic for lithium silicates were detected.

The XRD pattern of 50.8 wt.% $LiCl/SiO_2$ catalyst after calcination in air at 550°C (Fig. 4D) contain diffraction peaks of LiCl, peroxide Li_2O_2 and the residual silica (marked by arrow). Therefore, the XRD results are evident for partial conversion of LiCl at the catalysts surface to Li_2O_2 phase. Furthermore, full conversion of $DyCl_3$ to DyOCl was registered. Both oxygen-containing phases formed during calcination are stable at least at 550°C, and in contrast to Li_2O, do not react with silica at this temperature. The oxygen adsorption by supported metal-chlorides detected in TPO–TP-reaction experiments (Figs. 2 and 3) could be attributed to the formation of those phases.

The strong peak of Li_2O_2 (at $2q = 35.0°$) and 2 0 0 reflection of LiCl ($2q = 34.88°$) are overlapping. Therefore, formation of Li-peroxide in $LiCl/SiO_2$ catalyst after calcination in air at 550°C was confirmed by laser Raman scattering spectroscopy (LRS). It is well-established that O–O stretch vibration in alkali or alkaline-earth metal peroxides that cannot be observed in infrared spectra produces intense bands in Raman spectra at frequency region of 750–850 cm^{-1} [21]. Li_2O_2 exhibits a band at Raman shift of 790 cm^{-1} [21], Raman spectra of pure silica support and 50.8 wt.% $LiCl/SiO_2$ catalyst after calcination in air at 550°C are shown in Fig. 5. The spectra of silica support exhibits a peak centered at about $791 \pm 1\ cm^{-1}$ that could be attributed to in-plane bending of Si–O–Si groups in silica crystals (v_2 vibration mode) [22]. The spectra of calcined $LiCl/SiO_2$ catalyst exhibits two peaks: one at about $790 \pm 1\ cm^{-1}$ that disappears in time after exposure of the sample to ambient atmosphere for more than 20 min leaving the other one at $791 \pm 1\ cm^{-1}$ characteristic of silica support. The spectra characteristic for calcined LiCl phase at the surface of silica support is displayed in the bottom of Fig. 5 as a difference of the corresponding intensities measured with $LiCl/SiO_2$ and pure silica clearly elucidating the Raman features of Li_2O_2 phase. It is similar to that measured with pure Li_2O_2 phase and reported in [21]. The negative feature is spurious and within the error as shown in Fig. 5. The peak at $790 \pm 1\ cm^{-1}$ is attributed to O–O stretch vibration in O_2^{2-} peroxo-anions of Li_2O_2 phase formed by reaction of LiCl with oxygen during calcination. The Raman spectra are in agreement with XRD data.

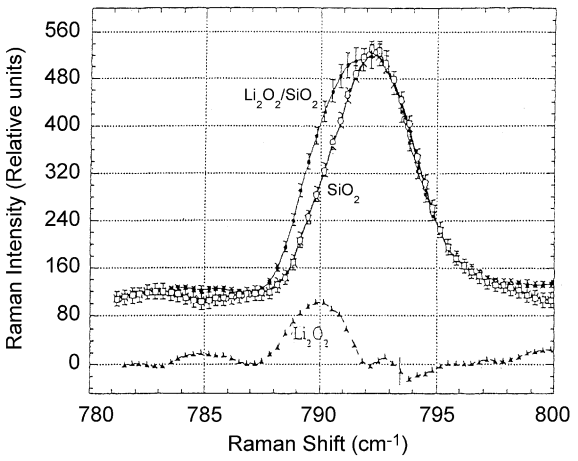

Fig. 5. LRS spectra of pure silica support (SiO_2) and 50.8 wt.% $LiCl/SiO_2$ catalyst calcined in air at 550°C (Li_2O_2/SiO_2).

Appearance of Li-peroxide phase after exposure of supported LiCl to oxygen at ODH conditions reported by Gutman et al. [17] for $LiCl/SiO_2$, Wang et al. [16] for $LiCl/ZrO_2$ and recently by Bothe-Almquist et al. [18] for LiCl/MgO contradicts a well-established fact of low thermostability of this phase. All authors detected sharp diffraction lines corresponding to Li_2O_2 phase whose crystal domain size determined using Sherrer equation was 5–7 nm. These XRD patterns were obtained after cooling the catalyst samples to room temperature, so that existence of this phase at ODH conditions is questionable. But formation and

stability of Li_2O_2 phase at ODH conditions follows from our TPO–TPD data measured with $LiCl/SiO_2$ catalyst. The oxygen consumption that only leads to the formation of a new oxide phase was detected at temperatures >400°C (Fig. 2). Further cooling in He flow to room temperature as well as subsequent re-exposing of the sample to oxygen in repeated TPO experiment was not accompanied by evolution/consumption of any gaseous products. It excludes the possibility of formation/decomposition of the Li_2O_2 phase by cooling or short exposure to oxygen at low temperature. As mentioned above, in our experiments the exposure of cooled samples to oxygen and ambient moisture was avoided before recording the XRD and RLS patterns that excluded the possibility of further phase transformations.

According to Refs. [19,20] Li_2O_2 crystals dissociate at oxygen pressure of 1 atm and 194°C, and should be fully decomposed at 550°C and ambient atmospheric pressure. Even if oxidation of LiCl with oxygen produces a phase with structure close to Li_2O_2 (XRD) containing –O–O– peroxo-anions (LRS), this phase is probably modified to increase its thermal stability. Information on possible modification of Li_2O_2 phase, produced during LiCl oxidation, was measured by XPS. The XPS spectra of silica support, Li_2O_2 (Aldrich), Li_2O/SiO_2 (calcination of $LiNO_3/SiO_2$, 550°C) and $LiCl/SiO_2$ calcined in air at 550°C in BE range corresponding to O 1s core are shown in Fig. 6.

Silica exhibits a symmetric peak centered at BE of 532.6 eV characteristic of only one state of oxygen atoms in the surface layer. Introduction of Li_2O that partially reacted with silica forming lithium silicates only slightly affected the peak maximum position (BE, 532.7 eV). Li_2O_2 phase was characterized also by one symmetric peak, centered at lower BE of 530.9 eV. Oxidation of LiCl at silica surface produces a catalyst whose XPS spectra consists of three components (Fig. 6). They represent different forms of surface oxygen atoms characteristic of silica support (BE, 532.7 eV) and two additional oxygen states (BE, 531.6 and 530.0 eV) produced during calcination of $LiCl/SiO_2$ whose relative areas are 63.3, 31.6 and 19.9%, respectively.

Existence of these two last oxygen states at the surface of oxidized $LiCl/SiO_2$ catalyst could be explained as a result of modification of Li_2O_2 phase by chlorine. Interaction of Li_2O_2 crystals with remained LiCl phase

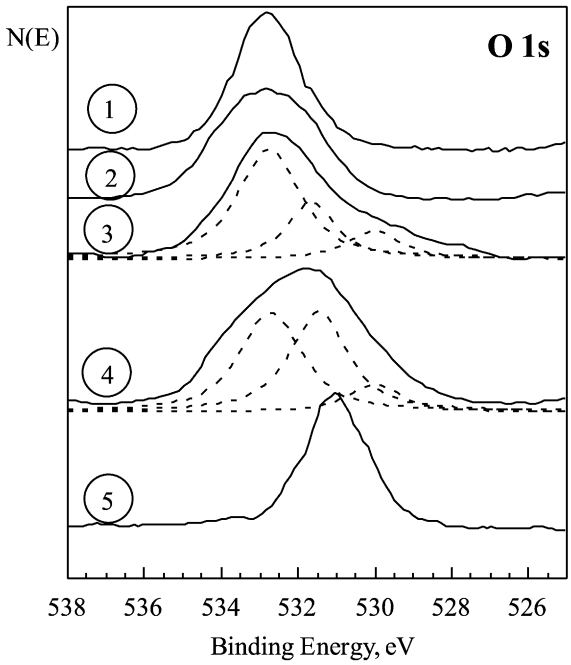

Fig. 6. XPS spectra: (1) pure silica support; (2) silica-supported catalysts calcined in air at 550°C, 33.2 wt.% Li_2O/SiO_2; (3) 50.0 wt.% $LiCl/SiO_2$; (4) 39.0 wt.% LiCl–33.7 wt.% $DyCl_3/SiO_2$; (5) individual Li_2O_2 phase.

could produce a protective layer $Li_2O{\cdot}LiCl$ at the surface of Li_2O_2 crystals as a result of partial O^-–Cl^- substitution that increases the temperature where the Li_2O_2 decomposition oxygen pressure reaches 1 atm. This splits the single band in XPS spectra corresponding to oxygen atoms in Li_2O_2 into two bands corresponding to surface oxychloride species $Li_2O{\cdot}LiCl$ and modified Li_2O_2 surface. Addition of $DyCl_3$ to $LiCl/SiO_2$ fully converted to DyOCl (XRD) after calcination, strongly increased the intensity of the peak corresponding to O 1s core with BE 531.6 eV (Fig. 6) and did not affect the peak at BE 530.0 eV. It redistributed the relative areas of the peaks corresponding to three forms of surface oxygen: 45.0% (BE 532.7 eV), 43.8% (BE 531.6 eV) and 11.2% (BE 530.0 eV). This confirms that the peak at BE of 531.6 eV in XPS spectra of oxidized $LiCl/SiO_2$ sample is related to O 1s core in oxychloride species.

Modification of Li_2O_2 phase by chlorine due to partial substitution of O^- for Cl^- results in expansion of the Li_2O_2 lattice. Simulation of XRD patterns of

Li-peroxide phase after progressive O^-–Cl^- substitution carried out by using DBWS-9807 Rietveld program showed that increasing the substitution extent from 0 to 5% and then to 10% should shift all the peaks to lower diffraction angles. The positions of Li_2O_2 diffraction lines in $LiCl/SiO_2$ catalyst calcined in air at 550°C (Fig. 4D) corresponded to zero substitution extent. We suppose that Li_2O_2 formed by oxidation of LiCl is modified by chlorine in a way described above so that Li-oxychloride species modifying Li_2O_2 are formed in a thin layer at the surface of Li-peroxide crystals. This explains all our observations taking into account that XPS gives information on the particles surface layer while XRD on their bulk structure:

- Appearance of the bands corresponding to large Li_2O_2 crystals in XRD spectra and Raman shift in LRS spectra corresponding to O–O stretch vibration.
- Splitting of single peak corresponding to O 1s core in XPS spectra of Li_2O_2 into two peaks with different BE in XPS spectra of calcined $LiCl/SiO_2$.
- Increasing the thermostability of Li_2O_2 crystals in calcined $LiCl/SiO_2$ as a result of decreasing their dissociation oxygen pressure due to the formation of such protective modified surface layer.

3.2.3. Dynamics of active phases in LiCl-based catalysts

The TPO–TP-reaction experiments with butane demonstrated a close linkage between reversible oxygen adsorption by $LiCl(DyCl_3)/SiO_2$ catalysts and their activity in ODH. XRD and XPS spectra of calcined 50.8 wt.% $LiCl/SiO_2$ sample were recorded after its reduction with butane at 550°C and further reoxidation at the same temperature to clarify the role of different oxygen species at the surface of oxidized LiCl catalysts in catalytic cycle. Comparison of XRD patterns of calcined and reduced catalyst shown in Fig. 4D and E exhibited substantial decrease of Li_2O_2/LiCl phase ratio after reduction. Reduction also caused appearance of lithium silicate (Li_2SiO_3) as it was observed in Fig. 4E. Reduction completely removed the peak at BE of 530.0 eV corresponding to O 1s core from XPS spectra of 50.8% $LiCl/SiO_2$ catalyst and substantially reduced the intensity of the peak at BE 531.6 eV (Fig. 7). They were attributed to modified Li_2O_2 and Li_2O·LiCl species

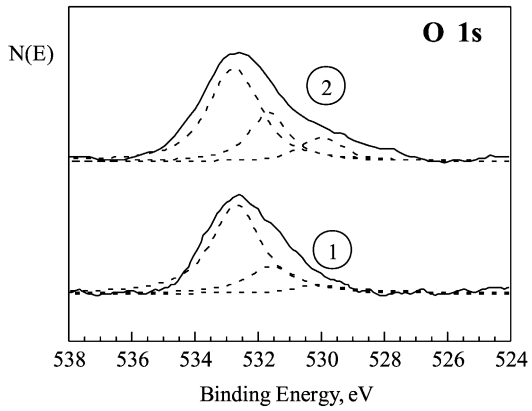

Fig. 7. XPS spectra: (1) 50.0% $LiCl/SiO_2$ catalyst calcined in air at 550°C after reduction by C_4H_{10} at 550°C; (2) after *n*-C_4H_{10} reduction–air reoxidation at 550°C.

at the surface of Li_2O_2 crystals, respectively. It follows from those data that oxidized LiCl (Li_2O·LiCl, Li_2O_2) reacts with butane preferentially through the oxygen atoms that belong to Li_2O_2 phase and partially by oxygen atoms in oxychloride species. This destroys the Li_2O·LiCl layer at the surface of Li_2O_2 crystals decreasing their thermostability, so that part of them decompose to Li_2O that reacts with silica support forming lithium silicate.

Reoxidation increased the Li_2O_2/LiCl phase ratio again as it is shown in Fig. 4F. It also caused appearance of the band at BE of O 1s electrons of 530.0 eV and increased the intensity of BE 531.6 eV band in XPS spectra (Fig. 7). Therefore, XPS spectra of reoxidized catalyst became similar to the freshly calcined sample (Fig. 6). It means that lithium chloride remaining after reduction at silica surface reacts with oxygen at reoxidation step forming Li_2O_2 particles modified on the surface layer by Li_2O·LiCl. Those data allow us to propose a scheme representing the dynamics of active phases in $LiCl/SiO_2$ catalyst during the *n*-butane ODH catalytic cycle shown in Fig. 8. LiCl reversibly interacts with oxygen from the gas phase forming Li_2O_2 crystals modified by Li_2O·LiCl at surface layer. The butane molecule reacts with oxygen ions mainly of Li_2O_2 phase (probably O^- ions of $[Li^+O^-]$ centers detected recently in Li_2O_2/MgO by ESR [18]) yielding light C_2–C_4 olefins, CO/CO_2 and water evolution. The $[Li^+O^-]$ are considered in Li–MgO-based catalysts as most probable active sites

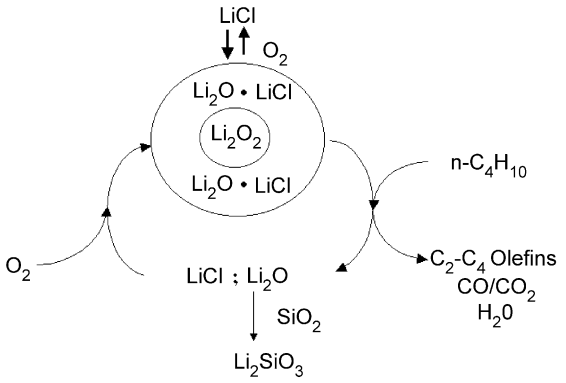

Fig. 8. Proposed active phases dynamics in $LiCl/SiO_2$ catalyst during *n*-butane ODH.

for hydrogen abstraction from hydrocarbons followed by production of olefins and complete combustion products [22–25]. This produces LiCl that reacts with oxygen closing the catalytic cycle, and Li_2O that reacts irreversibly with silica support forming stable lithium silicate phase. Formation of Li-silicate eliminates the active lithium from catalytic cycle, more pronounced at higher temperatures, a reason for catalysts deactivation. Dysprosium chloride after oxidation forms DyOCl phase that also contains dynamic oxygen atoms participating in catalytic cycle.

One of the consequences of active phase dynamics shown in Fig. 9 should be a substantial increase of the stability of LiCl catalyst in butane ODH after replacing the silica support for MgO that cannot react with lithia to form a stable phase. The MgO support was impregnated with LiCl solution as described above for deposition of LiCl on silica. The catalyst containing 10.0 wt.% LiCl after drying at 120°C was calcined in air at 550°C for 16 h. XRD patterns of this sample (not shown) were evident for partial conversion of LiCl into Li_2O_2 phase during calcination. The patterns of XPS spectra (not shown) were similar to that recorded for calcined $LiCl/SiO_2$. Testing the LiCl/MgO catalyst in butane ODH at standard conditions (600°C) displayed higher initial hydrocarbon conversion compared with 50.0 wt.% $LiCl/SiO_2$ in agreement with the results measured at 550°C (Fig. 1). Fig. 9 presents butane conversions and C_2–C_4 olefins selectivity measured with 10.0 wt.% LiCl/MgO and 50.0 wt.% $LiCl/SiO_2$ at 600°C over periods up to 100 min of run. The activity

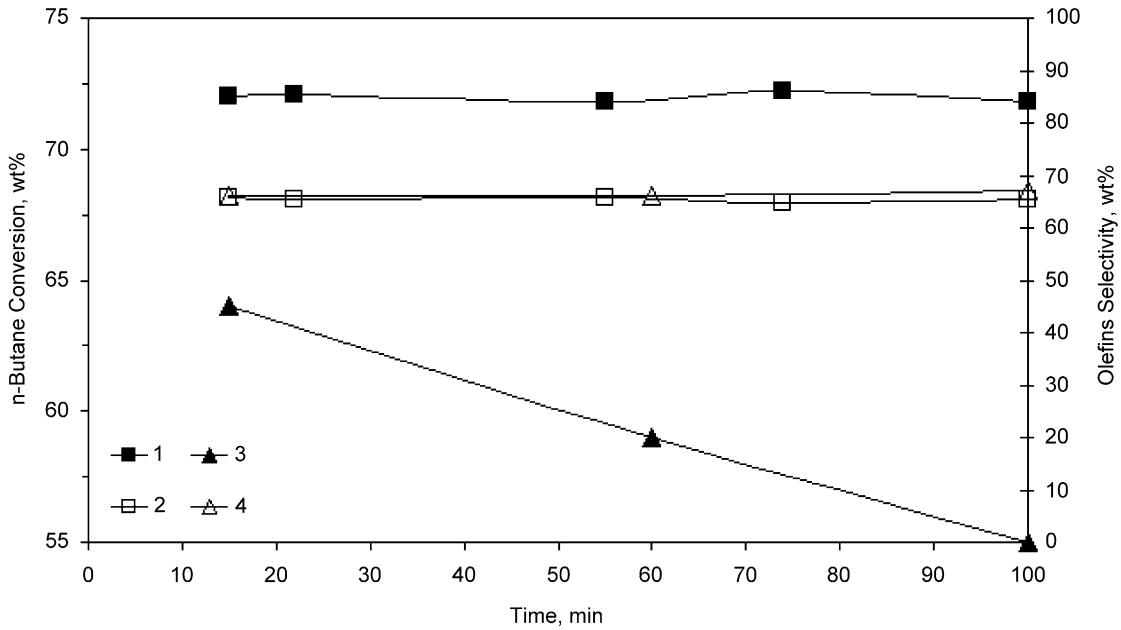

Fig. 9. Stability of $LiCl/SiO_2$ and LiCl/MgO catalysts performance in *n*-butane ODH (conditions as in Fig. 1): 10.0 wt.% LiCl/MgO — (1) *n*-butane conversion, (2) olefins selectivity; 50.0 wt.% $LiCl/SiO_2$ — (3) *n*-butane conversion, (4) olefins selectivity.

of LiCl/MgO catalyst remained unchanged during all the testing period while $LiCl/SiO_2$ catalyst displayed substantial deactivation. The LiCl/MgO catalyst with optimal LiCl loading displayed about twice higher olefins productivity compared with that reported in [13] for *n*-butane ODH with Cl-promoted multioxide catalyst Li_2O–Dy_2O_3–Cl/MgO.

4. Conclusions

Supported LiCl displays the highest activity and selectivity in butane ODH among eight alkali metal halides. Addition of $DyCl_3$ to supported LiCl increases the olefins yield due to higher butane conversion. LiCl on the surface of SiO_2 or MgO adsorbed oxygen at temperature >400°C and became partially converted to Li_2O_2 crystals detected by XRD and RLS with domains size of 5–7 nm. XPS results suggested that those Li_2O_2 crystals are decorated by a protective layer including Li_2O·LiCl species that could be formed due to surface reaction between Li_2O_2 and LiCl phases. The results of separate TP-reaction experiments (catalysts O_2-oxidation–butane reduction) together with XRD, RLS and XPS measurements showed that butane at ODH conditions reacted mainly with oxygen species of Li_2O_2 phase probably attributed to $[Li^+O^-]$ pairs. Part of Li_2O produced in reaction-reoxidation cycle reacted with SiO_2 support forming Li-silicates that caused irreversible deactivation. Such interaction did not occur on MgO support that displayed high stability of LiCl/MgO catalyst. The high yield of C_2–C_3 olefins of ∼50% measured with LiCl/MgO catalyst and negligible chlorine release in short runs imply the significance of further testing the long-time stability of this catalyst and of possible corrosion problems in potential application.

References

[1] M. Huff, L.D. Schmidt, J. Phys. Chem. 97 (1993) 1185.
[2] M. Huff, L.D. Schmidt, J. Catal. 149 (1994) 127.
[3] M. Huff, L.D. Schmidt, J. Catal. 155 (1995) 82.
[4] M. Huff, L.D. Schmidt, AIChE J. 42 (1996) 3484.
[5] A. Beretta, E. Ranzi, P. Forzatti, Catal. Today 64 (2001) 103.
[6] A. Beretta, E. Ranzi, P. Forzatti, Chem. Eng. Sci. 56 (3) (2001) 779.
[7] B. Delmon, Stud. Surf. Sci. Catal. 110 (1997) 43.
[8] R.K. Grasselli, Catal. Today 49 (1999) 141.
[9] D.B. Fox, E.H. Lee, CHEMTECH 3 (3) (1973) 186.
[10] F. Cavani, F. Trifiro, Catal. Today 24 (1995) 307.
[11] M.V. Landau, M.L. Kaliya, M. Herskowitz, P.F. van den Oosterkamp, P.S.G. Bocque, CHEMTECH 26 (2) (1996) 24.
[12] C.J. Conway, D.J. Wang, J.H. Lunsford, Appl. Catal. 79 (1991) L1.
[13] M.V. Landau, M.L. Kaliya, A. Gutman, L.O. Kogan, M. Herskowitz, P.F. van den Oosterkamp, Stud. Surf. Sci. Catal. 110 (1997) 315.
[14] M. Herskowitz, M.V. Landau, M. Kaliya, EP 804287 A1, 1995.
[15] S. Wang, K. Murata, T. Hayakawa, S. Hamakawa, K. Suzuki, Energy Fuels 14 (2000) 899.
[16] S. Wang, K. Murata, T. Hayakawa, S. Hamakawa, K. Suzuki, Catal. Lett. 59 (1999) 173.
[17] A. Gutman, M.V. Landau, M.L. Kaliya, M. Herskowitz, in: Fourth European Congress on Catalysis, EUROP-CAT-IV, Riminy, Italy, September 5–10, 1999, Book of Abstracts, p. 37.
[18] C.L. Bothe-Almquist, R.P. Ettireddy, A. Bobst, P.G. Smirniotis, J. Catal. 192 (2000) 174.
[19] M. Blumental, Roczniki Chem. 12 (1932) 119.
[20] G.A. Slack, S. Mroczkowski, J. Solid State Chem. 107 (1993) 489.
[21] H.H. Eysel, S. Thym, Z. Anorg. Allg. Chem. 411 (1975) 97.
[22] E. Astorino, J.B. Peri, R.J. Wiley, G. Busca, J. Catal. 157 (1995) 482.
[23] T. Ito, J.-X. Wang, C.-H. Lin, J.H. Lunsford, J. Am. Chem. Soc. 107 (1985) 5062.
[24] C.-H. Lin, T. Ito, J.-X. Wang, J.H. Lunsford, J. Am. Chem. Soc. 109 (1987) 4808.
[25] P.J. Gellings, H.J.M. Bouwmeester, Catal. Today 58 (2000) 1.